Interfacial Adsorption and Dynamics of Fluorotelomers with Soil Minerals – Mechanistic Insights

*Narasimhan Loganathan, Libby Ashby, Christina E. Schumm and Angela K. Wilson**

Department of Chemistry and the MSU Center for PFAS Research, Michigan State University, East Lansing, Michigan 48824, United States

*) **Corresponding author's email:** akwilson@msu.edu
Includes: Figures: 13, Table – 2

Surface construction:

The external surface of kaolinite, montmorillonite and illite were constructed by cleaving the structure along the (001) plane at the middle of the interlayer region. This cleaving procedure yielded two different basal surfaces for kaolinite: (i) a hydrophilic surface having hydroxyl groups; and (ii) a hydrophobic siloxane surface. Because of the 2:1 structure, the resulting basal surfaces of montmorillonite and illite have only their hydrophilic Si/Al tetrahedral layers exposed to the mesopore region. Importantly, after cleavage, each basal surface of the 2:1 mineral retains only one-half of the charging balancing cations. The total thickness of clay minerals is ~12 Å, ~20 Å and ~16 Å for kaolinite, montmorillonite and illite, respectively. Regardless of the mineral substrate, the simulation cell consists of two clay layers with the mesopore regions saturated with bulk water density (~20,000 H_2O molecules) with 16 6:2 FTS or 6:2 FTC molecules. The PFAS molecules were distributed into distinct regions of the H_2O saturated mesopore regions and are also separated from each other by ~20-25 Å. A schematic illustration of the simulated montmorillonite with 6:2 FTS at time t=0 *ns* is shown in Figure S1c.

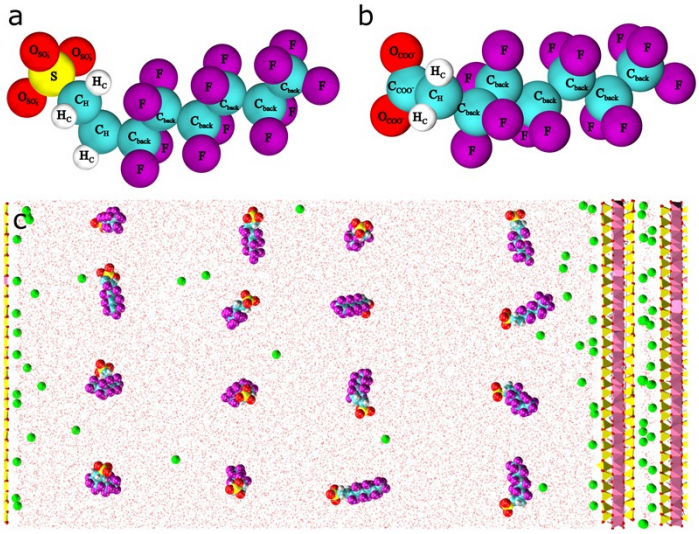

Figure S1: Pictorial representation of atom types associated to (a) FTS and (b) FTC and (c) schematic representation of simulated 6:2 FTS – montmorillonite model at time t= 0 ns. Color codes: yellow – Si tetrahedra; pink – Al octahedra/tetrahedra; green spheres – Ca ions; yellow spheres – S; cyan spheres – C

(carbons bonded to H: C_H; carboxyl carbon: C_{COO^-}; backbone carbon C_{back}); white spheres – H (hydrogens bonded to carbon: H_C); purple spheres – F; red spheres – O (sulfonic oxygens $O_{SO_3^-}$ and carboxyl oxygens O_{COO^-}). H_2O molecules are shown in dotted representation.

Table S1: The cell dimensions used in the NVT (post-NPT) simulation runs for 6:2 FTS and 6:2 FTC systems in all three clay minerals are provided.

Clay		L_x	L_y	L_z
Kaolinite	**6:2 FTS**	**62.26**	**71.64**	**148.59**
	6:2 FTC	62.30	71.71	148.17
Montmorillonite	**6:2 FTS**	**62.25**	**71.86**	**148.83**
	6:2 FTC	62.20	71.95	149.93
Illite	**6:2 FTS**	**62.14**	**71.66**	**149.36**
	6:2 FTC	62.17	71.67	148.54

Atomic Density Profiles

Ca^{2+} ions

The ADP's of Ca^{2+} ions as functions of the distance normal to the basal surface vary substantially between the mineral surfaces. All Ca^{2+} ions were associated with the hydrophobic siloxane region of kaolinite at distances of ~4.5 Å away from the surface (Figure 1c). In contrast, the ADP's of Ca^{2+} ions in montmorillonite are composed of two peaks at distances ~2.1 Å and ~4.5 Å away from the basal surface representing inner- and outer-sphere coordination, respectively (Figure 2b and 2c). Due to the highly charged illite surface, almost all Ca^{2+} ions are adsorbed at the basal surface at distances ~0.7 Å and ~2.1 Å away from the surface. Both the peaks exhibit inner-sphere coordination: (i) center of ditrigonal cavities; (ii) on top of the substituted tetrahedra (Figure 3b and 3c). The reported ADP's of Ca^{2+} are in good agreement with our previous studies.[1,2]

H_2O

As for Ca^{2+} ions, the ADP's of H_2O molecules as functions of the distance normal to the basal surface of clay minerals are not influenced by the presence of surface bound 6:2 FTS and 6:2 FTC molecules. However, it is evident from Figures 1a-1f that interfacial adsorption of H_2O molecules varies substantially between the three mineral surfaces. For instance, the O_{H2O} molecules exhibit three peaks (~2.5, 4.1 and 6.4 Å) at the hydroxyl surface of kaolinite, while there are only two prominent peaks (~2.7 Å and ~5.6 Å) at the siloxane surface of kaolinite along with a broad shoulder between ~3.0-4.5 Å. The well-defined peaks near the hydroxyl surface stem from the strong H-bonding interactions between 'H' of the surface hydroxyl groups and the O_{H2O}. In contrast, due to the hydrophobic character of the siloxane surface, the H_2O molecules typically exhibit broad distributions as shown in previous studies.[2,3]

It is evident from Figure 2 that the O_{H2O} exhibits three peaks at distances ~2.7, 4.6 and 6.3 Å away from either basal surface of montmorillonite, irrespective of the fluorotelomer molecules. The presence of the H_{H2O} peak at ~1.7 Å near the basal surface demonstrates that the surface adsorbed H_2O molecules are coordinated through only one of their H_{H2O} atoms which is in good agreement with previous studies. On the other hand, the H_2O molecules in illite show four distinct and well-defined peaks for O_{H2O} at distances ~2.6, 4.6, 5.3 and 6.5 Å from the basal surfaces along with a prominent shoulder at ~1.8 Å (Figure 3). As shown in previous studies, the H_2O molecules are coordinated to the basal surface of illite, however, in two different configurations. The O_{H2O} molecules closest to the surface (~1.8 Å) are located at the center of ditrigonal cavities with both

their H_{H2O} atoms coordinating with the basal surface oxygen atoms. In contrast, the O_{H2O} peak at 2.6 Å is located above the substituted Al tetrahedra and is coordinated through only one H-bonds to the surface. Importantly, irrespective of the clay minerals, the reported H_2O interfacial adsorption is similar to previous studies at relevant thermodynamic conditions.[2–4]

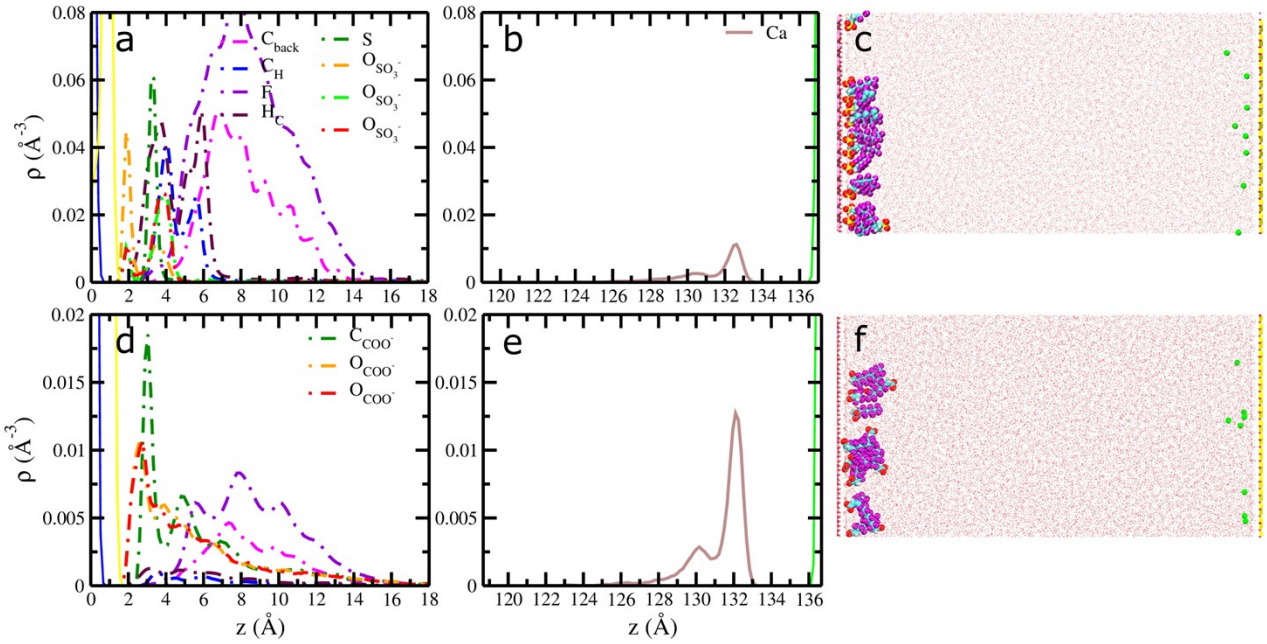

Figure S2: Computed ADPs of 6:2 FTS, 6:2 FTC and Ca^{2+} ions as functions of distance relative to surface normal of kaolinite. (a, b) – 6:2 FTS; (d, e) - 6:2 FTC. Schematic representation of 6:2 FTS (c) and 6:2 FTC (f) with kaolinite system at the end of data production run. Distance 0 is the mean position of hydroxyl 'O' atoms. ADP color codes: yellow – Si tetrahedra; pink – Al octahedra/tetrahedra; green spheres – Ca ions; yellow spheres – S; cyan spheres – C; white spheres – H; purple spheres – F; red spheres – O. H_2O molecules are shown in dotted representation.

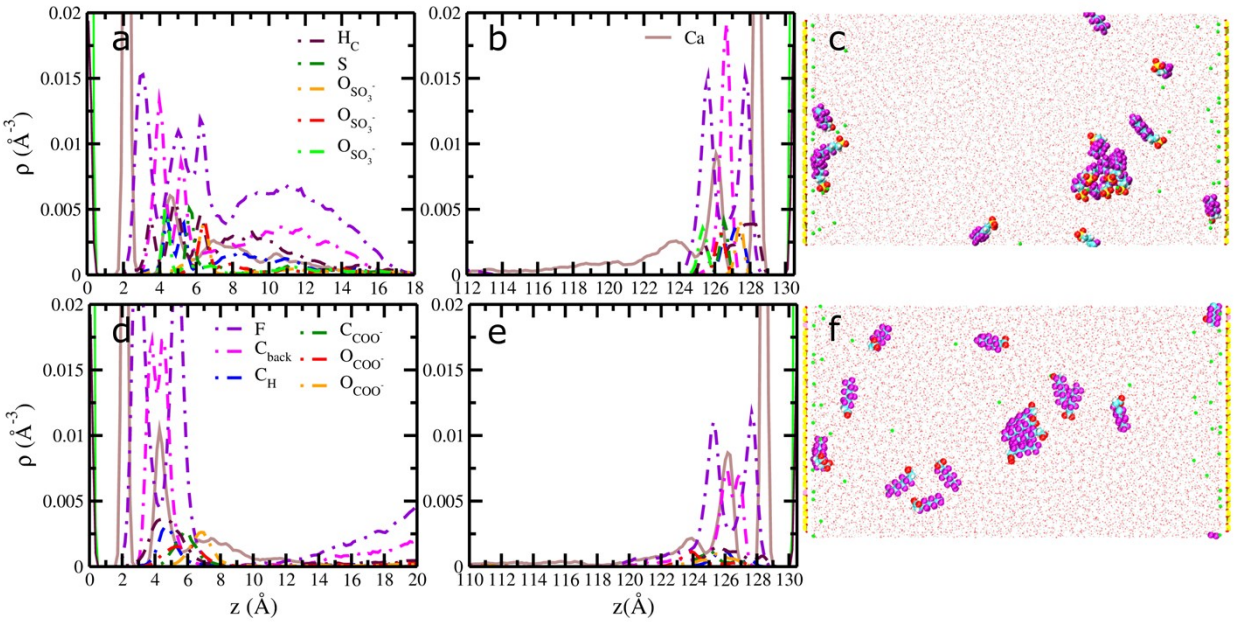

Figure S3: Computed ADPs of near surface interactions of 6:2 FTS, 6:2 FTC and Ca^{2+} ions as functions of distance relative to clay surface normal of montmorillonite. (a,b) - 6:2 FTS; (d,e) – 6:2 FTC. Schematic representations of 6:2 FTS (c) and 6:2 FTC (f) with montmorillonite system at the end of data production run. Distance 0 is the mean position of tetrahedral 'O' atoms. ADP color codes: yellow – Si tetrahedra; pink – Al octahedra/tetrahedra; green spheres – Ca ions; yellow spheres – S; cyan spheres – C; white spheres – H; purple spheres – F; red spheres – O. H_2O molecules are shown in dotted representation.

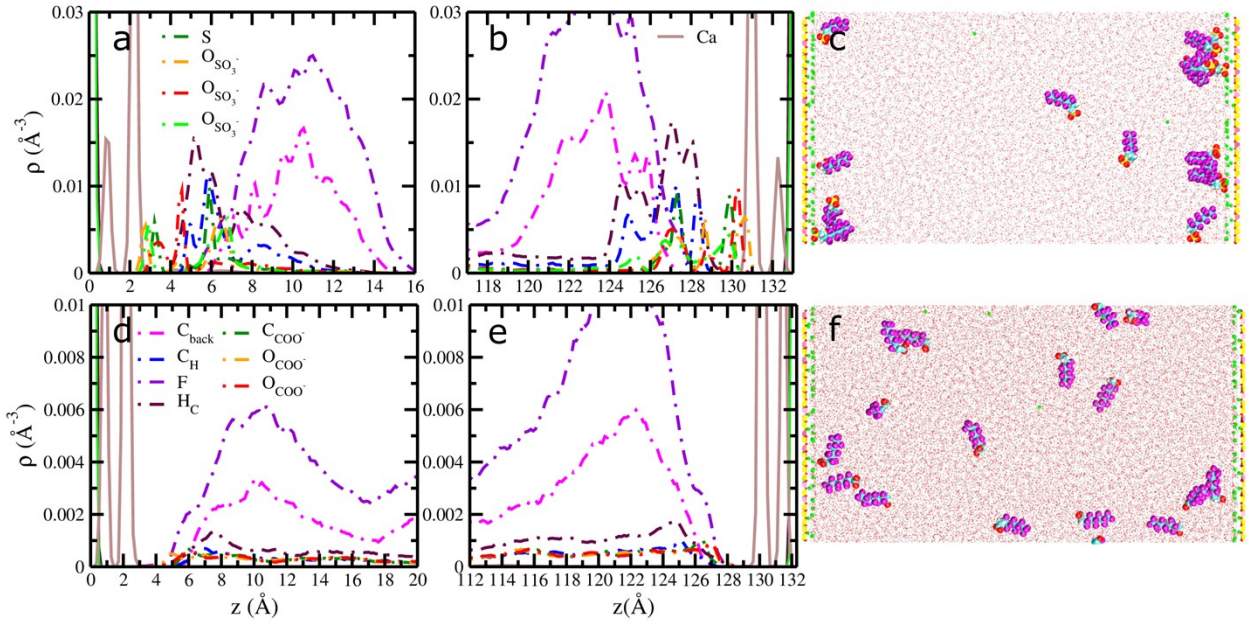

Figure S4: Computed ADPs of near surface interactions of 6:2 FTS, 6:2 FTC and Ca^{2+} ions as functions of distance relative to clay surface normal of illite. (a,b) - 6:2 FTS; (d,e) – 6:2 FTC. Schematic representations of 6:2 FTS (c) and 6:2 FTC (f) with illite system at the end of data production run. Distance 0 is the mean position of tetrahedral 'O' atoms. ADP color codes: yellow – Si tetrahedra; pink – Al octahedra/tetrahedra; green spheres – Ca ions; yellow spheres – S; cyan spheres – C; white spheres – H; purple spheres – F; red spheres – O. H_2O molecules are shown in dotted representation.

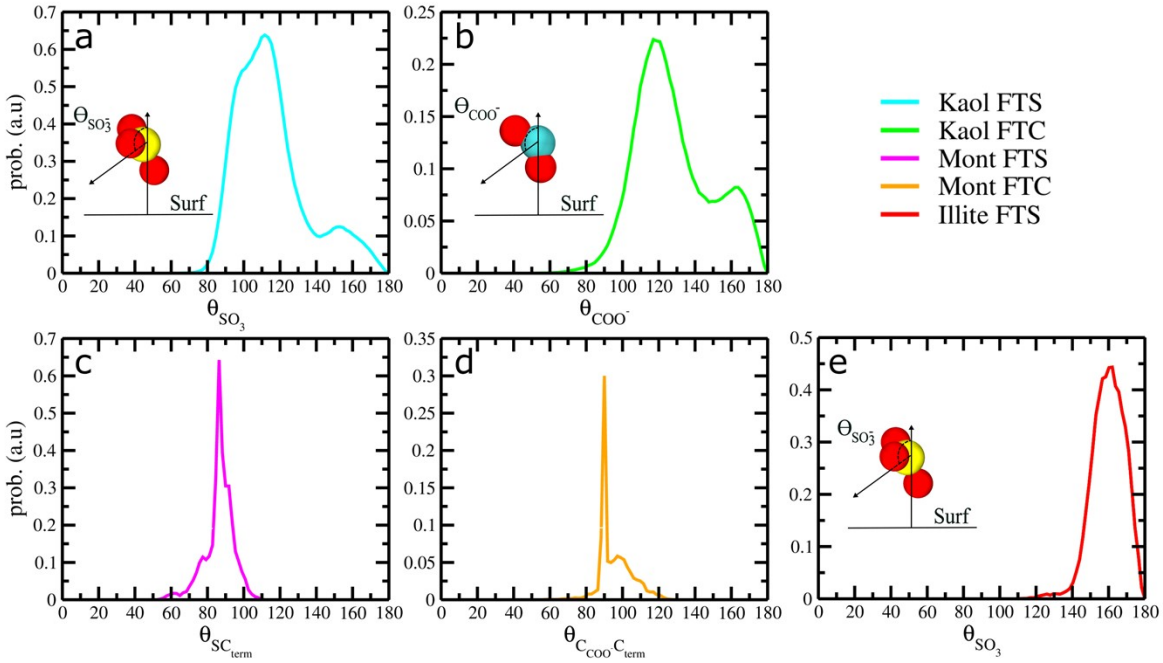

Figure S5: Computed orientation distributions of only the surface-adsorbed 6:2 FTS and 6:2 FTC at the basal surfaces of kaolinite (a,b), montmorillonite (c,d) and illite (e). θ_{SO3} is the angle between the vector bisecting the SO_3 groups of 6:2 FTS molecules with respect to the surface normal of a clay mineral (kaolinite/illite). θ_{COO^-} is the angle between the vector bisecting the COO^- groups of 6:2 FTC molecules with respect to the surface normal of kaolinite. θ_{SCterm} represents the angle between the vector made by the terminal S_{SO3} and the C_{CF3} of the backbone of 6:2 FTS molecules with respect to the surface normal of montmorillonite. $\theta_{CCOO\text{-}Cterm}$ represents the angle between the vector made by the terminal C_{COO} and the C_{CF3} of the backbone of 6:2 FTC molecules with respect to the surface normal of montmorillonite.

Orientation of surface adsorbed H_2O molecules:

The computed orientation of surface bound H_2O dipole vectors with respect to the surface normal shows completely different interfacial behavior between the three types of clay minerals (Figure S6). Importantly, the surface adsorbed water molecules are not influenced by the presence of 6:2 FTS/6:2 FTC molecules at the surface. For instance, the H_2O dipole vectors at the hydroxyl surface of kaolinite exhibit two peaks demonstrating the two different types of H_2O orientation (Figure S6a). The peak at ~ 22º represents H_2O dipole vectors pointed away from the basal surface while the peak at ~126º represents H_2O molecules with their dipole vectors pointed towards the hydroxyl surface exhibiting H-bonding interactions. In contrast, the H_2O molecules at the siloxane surface have their dipoles predominantly oriented at θ_1~54º which could be attributed to the hydrophobic character of the basal surface as shown in previous studies.[2,3] Similarly, the surface adsorbed H_2O molecules in montmorillonite predominantly have dipoles that are pointed towards their basal surface with a peak centered at ~120º. The peak at ~60º represents a similar H_2O orientation on the other basal surface of montmorillonite (Figure S6b). On the other hand, the H_2O dipole vectors in illite are largely oriented at ~160º which could be attributed to H_2O molecules located at the center of ditrigonal cavities and is consistent with our previous studies on PFAS (Figure S6c).[2] The peak at ~20º represents similar H_2O orientation on the basal surface of the other basal surface of illite.

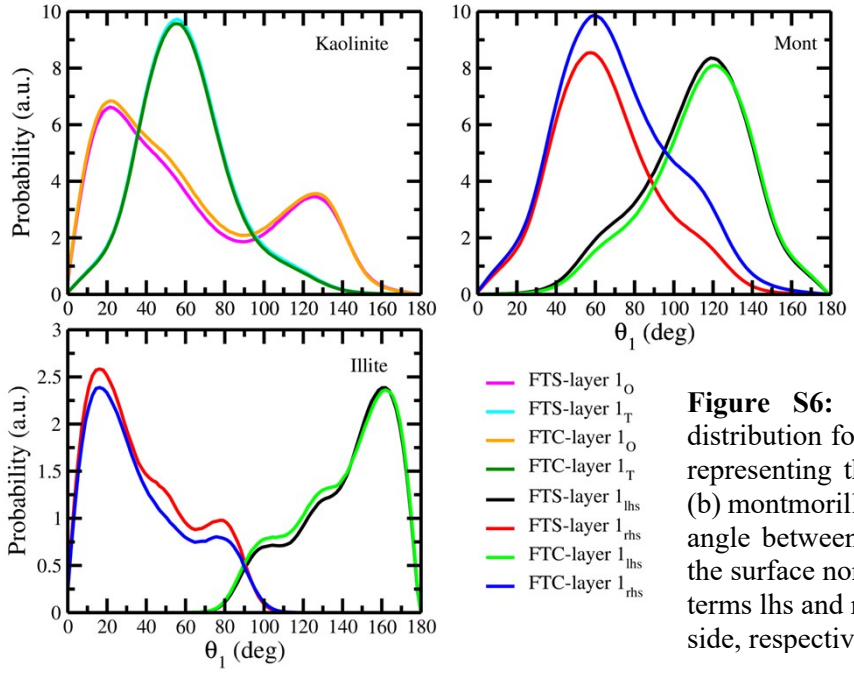

Figure S6: Calculated dipole orientation distribution for surface bound H_2O molecules representing the first layers on (a) kaolinite, (b) montmorillonite, (c) and illite surface. θ_1 is angle between the dipole vector of H_2O and the surface normal of each clay substrate. The terms lhs and rhs represent left and right-hand side, respectively.

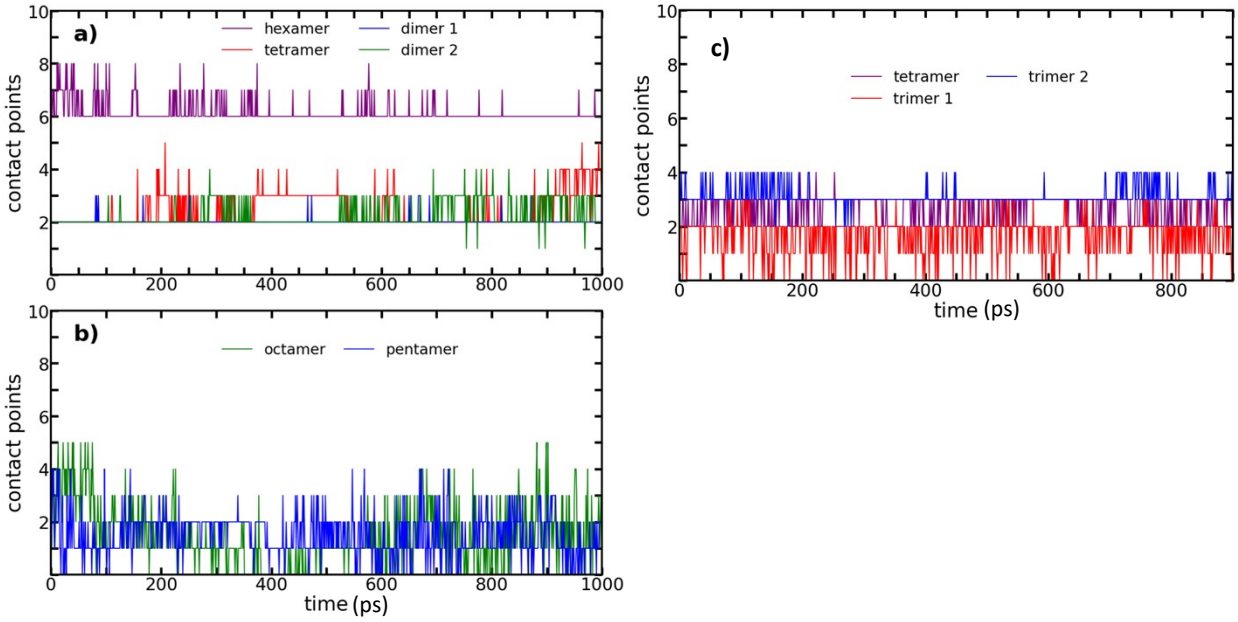

Figure S7: Average contact from each PFAS cluster with clay minerals as functions of time. (a) kaolinite – 6:2 FTS, (b) kaolinite – 6:2 FTC, (c) and illite – 6:2 FTC surface.

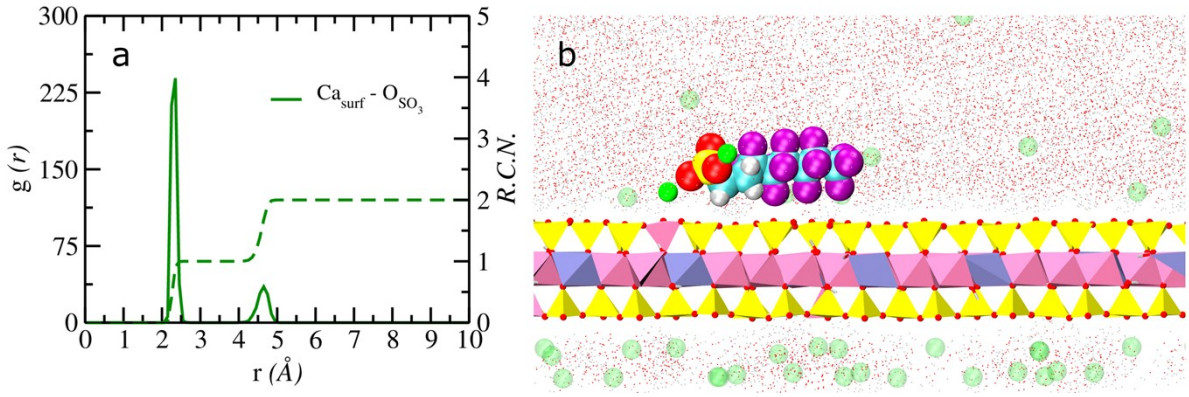

Figure S8: Pictorial representation of surface adsorbed 6:2 FTS coordinating to two different Ca^{2+} ions at the basal surface of montmorillonite. Color codes: yellow – Si tetrahedra; pink – Al octahedra/tetrahedra; gray – Mg octahedra; green spheres – Ca ions; yellow spheres – S; cyan spheres – C; white spheres – H; purple spheres – F; red spheres – O. Ca ions in transparent and H_2O molecules are shown in dotted representation.

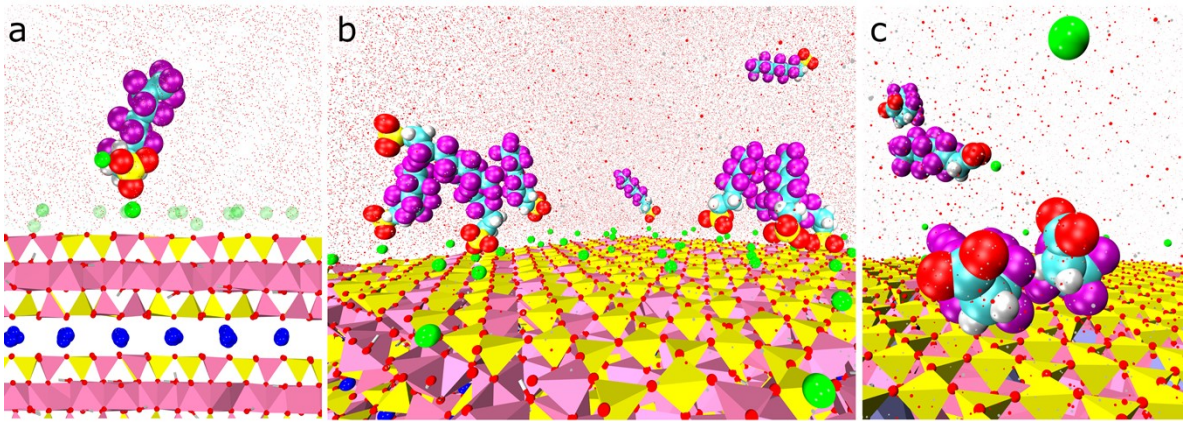

Figure S9: Pictorial representation of surface adsorbed 6:2 FTS coordinating to Ca^{2+} ions at the basal surface of illite and oriented perpendicular to the surface. a) 6:2 FTS coordinating to two different Ca^{2+} ions; b) 6:2 FTS molecules at one of the basal surfaces of illite. Color codes: yellow – Si tetrahedra; pink – Al octahedra/tetrahedra; green spheres – Ca ions; yellow spheres – S; cyan spheres – C; white spheres – H; purple spheres – F; red spheres – O. Ca ions in transparent and H_2O molecules are shown in dotted representation.

Interfacial coordination of Ca^{2+} ions

The coordination of Ca^{2+} ions vary significantly between montmorillonite and illite (Figure 2 and 3). The running coordination number (R.C.N.) numbers of Ca^{2+} ions with the basal surface oxygen (O_{surf}) atoms of montmorillonite are smaller than the corresponding values in illite (Figure S10a). This difference is primarily because the Ca^{2+} ions in montmorillonite are predominantly located on top of the substituted tetrahedral sites resulting in a value of ~2.0. In contrast, the ability of Ca^{2+} ions to adsorb both at the center of ditrigonal cavities and also on top of the substituted tetrahedral sites results in a higher R.C.N. of nearly 3.0. Since the Ca^{2+} ions are not influenced by the presence of kaolinite, their interfacial coordination behavior is not reported here.

It is evident from Figure S10b, that the coordination of Ca^{2+} with H_2O changes significantly between different clay minerals. For instance, the R.C.N. of Ca^{2+} is 8.0 which is consistent with

previous studies on bulk solution phases.[5] However, the R.C.N between Ca^{2+} and H_2O decreases to ~6.0 and ~5.0 in montmorillonite and illite, respectively. Such decreases in the R.C.N. are primarily due to the Ca^{2+} coordination with the basal surface oxygen atoms.

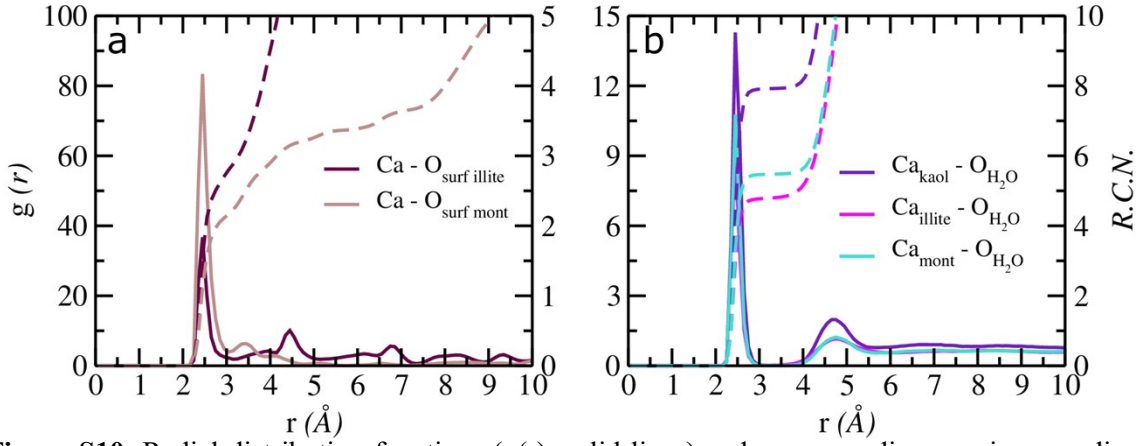

Figure S10: Radial distribution functions (g(r), solid lines) and corresponding running coordination number (RCN, dashed lines) for Ca^{2+} ions at the surfaces of montmorillonite and illite (a) and with H_2O molecules in kaolinite, montmorillonite and illite (b).

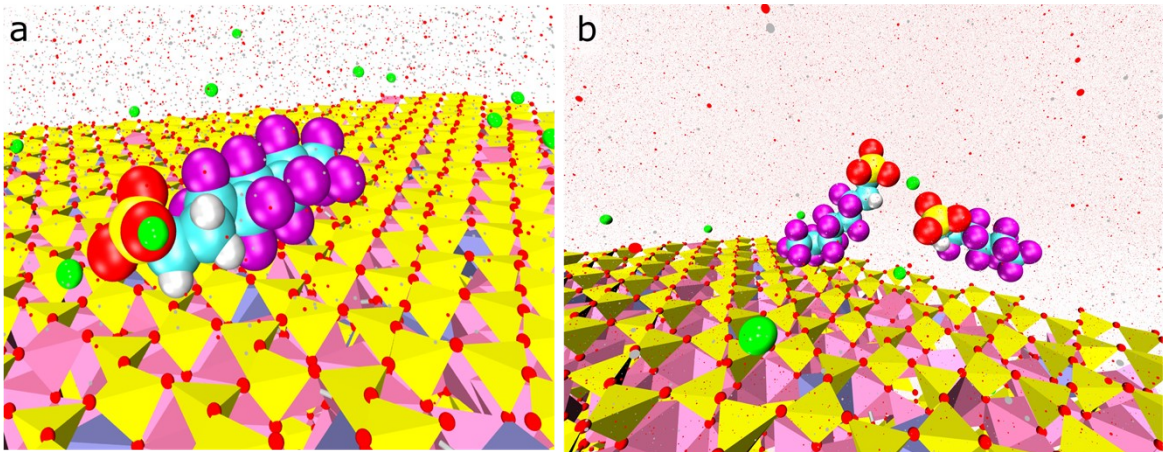

Figure S11: Pictorial representation of surface adsorbed 6:2 FTS (a) monomer coordinated to two different Ca^{2+} ions in montmorillonite; (b) dimer coordinated to Ca^{2+} ions away from the surface. For the sake of clarity, H_2O molecules are shown in dotted representation.

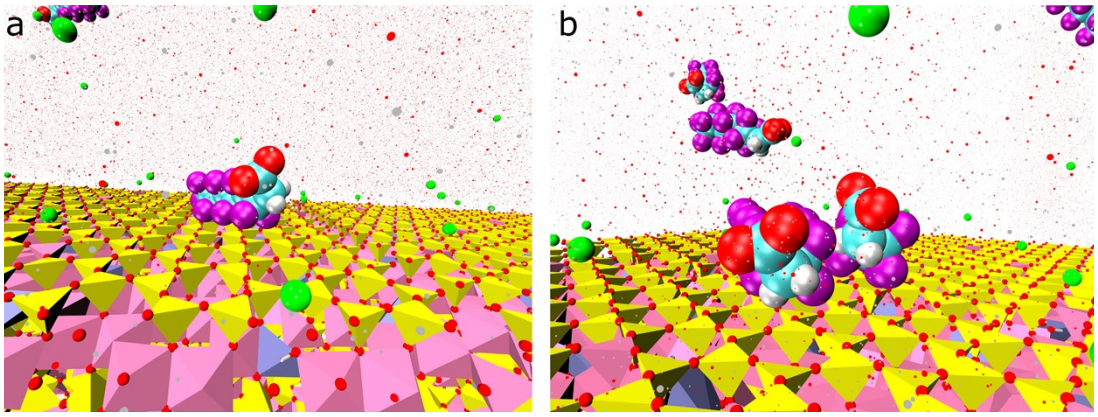

Figure S12: Pictorial representation of surface adsorbed 6:2 FTC a) monomer and b) dimer at the basal surface of montmorillonite. For the sake of clarity, H_2O molecules are shown in dotted representation.

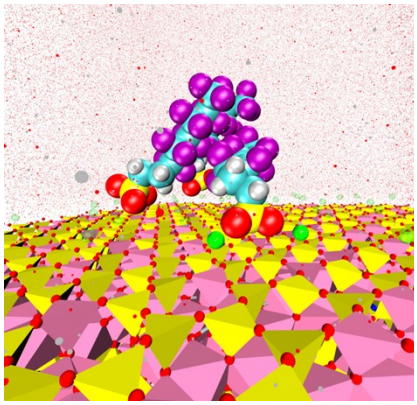

Figure S13: Pictorial representation of surface adsorbed 6:2 FTS trimer coordinated to two different Ca^{2+} ions at the basal surface of illite. For the sake of clarity, H_2O molecules are shown in dotted representation.

System	Avg	Mono.	Dim.	Trim.	Tetra.	Penta.	Hexa.	Octa.
Kaolinite - FTS	0.32	0.32 ± 0.02 (**2**)	0.63 ± 0.01 (**2**)	-	0.17 ± 0.01 (**1**)	-	0.15 ± 0.01 (**1**)	-
Kaolinite - FTC	2.20	0.48 ± 0.02 (**3**)	-	-	-	3.36 ± 0.03 (**1**)	-	2.13 ± 0.02 (**1**)
Montmorillonite - FTS	1.09	0.64 ± 0.01 (**2**)	1.53 ± 0.02 (**1**)	-	-	-	-	-
Montmorillonite - FTC	4.92	0.49 ± 0.12 (**1**)	7.10 ± 0.10 (**1**)	-	-	-	-	-
Illite - FTS	1.09	1.85 ± 0.02 (**3**)	-	0.44 ± 0.02 (**2**)	1.51 ± 0.02 (**1**)	-	-	-

Table S2: Mean and cluster-size dependent diffusion coefficients (10^{-10} m^2/s) of surface adsorbed 6:2 FTS and 6:2 FTC in all three clay minerals. The values in parentheses represent the number of clusters.

Further simulation and analysis details

The total energy (E_{tot}) for each system is computed as the sum of all intra- and intermolecular forces acting on each atom. Intramolecular potentials are harmonic for both bond stretches (E_{bonds}) and angle bending (E_{angles}), and the dihedral motion ($E_{dihedrals}$) is defined using a cosine series description. The intermolecular interactions are Coulombic interactions (E_{Coul}) and van der Waals forces (E_{vdW}). Interactions between different atom types are calculated with the Lorentz-Berthelot combination rules.

$$E_{tot} = E_{bonds} + E_{angles} + E_{dihedrals} + E_{Coul} + E_{vdW} \#(1)$$

Functional forms and parameters used for our simulations are obtained from ClayFF (including revised) and AMBER forcefields.[6,7]

All atomic density profiles provided in the main manuscript and SI are defined as the average count of atoms (N_{atom}) relative to clay surface normal. Atomic densities ($\rho_{atom}(z)$) are determined for each atom type in bins of size Δz z along the z-dimension and normalized by the total system volume (V).

$$\rho_{atom}(z) = \frac{\langle N_{atom}(\Delta z)\rangle}{V} \#(2)$$

Radial distribution functions were calculated as the average density of one atom type to another chosen reference type. The average number of atom type j are computed for radial distances relative to reference atom type i (r_{ij}), and is represented by $\langle N_{ij}\rangle$. The density of j atoms is represented by ρ

$$g(r_{ij}) = \frac{\langle N_{ij}\rangle}{4\pi\rho r_{ij}} \#(3)$$

Mean-square displacements were calculated for FT molecules and H_2O in each system to find diffusion coefficients, D. The dimensionality of the system is represented by d, while t is time and $\langle x^2\rangle$ is the mean-square displacement.

$$D = \frac{\langle x^2 \rangle}{2dt} \#(4)$$

References

1 B. F. N. W, *Brice F. Ngouana W.*, 2014.

2 C. E. Schumm, N. Loganathan and A. K. Wilson, Influence of Soil Minerals on the Adsorption, Structure, and Dynamics of GenX, *ACS ES&T Water*, 2023, **3**, 2659–2670.

3 N. Loganathan and A. K. Wilson, Adsorption, Structure, and Dynamics of Short- and Long-Chain PFAS Molecules in Kaolinite: Molecular-Level Insights, *Environ Sci Technol*, 2022, **56**, 8043–8052.

4 K. D. Papavasileiou, V. K. Michalis, L. D. Peristeras, M. Vasileiadis, A. Striolo and I. G. Economou, Molecular Dynamics Simulation of Water-Based Fracturing Fluids in Kaolinite Slit Pores, *Journal of Physical Chemistry C*, 2018, **122**, 17170–17183.

5 N. Loganathan, A. O. Yazaydin, G. M. Bowers, A. G. Kalinichev and R. J. Kirkpatrick, Cation and Water Structure, Dynamics, and Energetics in Smectite Clays: A Molecular Dynamics Study of Ca-Hectorite, *Journal of Physical Chemistry C*, 2016, **120**, 12429–12439.

6 J. Wang, R. M. Wolf, J. W. Caldwell, P. A. Kollman and D. A. Case, Development and testing of a general amber force field, *J Comput Chem*, 2004, **25**, 1157–1174.

7 R. T. Cygan, J. J. Liang and A. G. Kalinichev, Molecular models of hydroxide, oxyhydroxide, and clay phases and the development of a general force field, *Journal of Physical Chemistry B*, 2004, **108**, 1255–1266.